Nanoscale

Accepted Manuscript

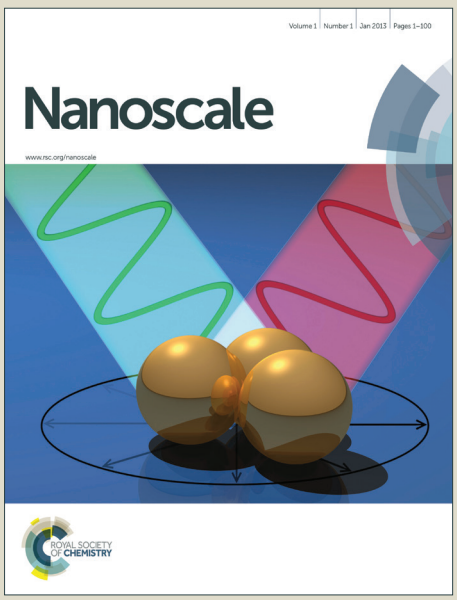

ROYAL SOCIETY OF CHEMISTRY

www.rsc.org/nanoscale

Cite this: DOI: 10.1039/c0xx00000x

www.rsc.org/xxxxxx

PAPER

Electrochemically induced Fenton reaction of few-layer MoS_2 nanosheets: Preparation of luminescent quantum dots via a transition of nanoporous morphology

Bang Lin Li,[a] Ling Xiao Chen,[a] Hao Lin Zou,[a] Jing Lei Lei,[b] Hong Qun Luo*[a] and Nian Bing Li*[a]

Received (in XXX, XXX) XthXXXXXXXXX 20XX, Accepted Xth XXXXXXXXX 20XX
DOI: 10.1039/b000000x

Electrochemically induced Fenton (electro-Fenton) reaction was used to the efficient and controllable preparation of hydroxyl radical, leading to the generation of luminescent quantum dots through the etching of as-exfoliated MoS_2 nanosheets. The observable morphologic changes of MoS_2 nanosheets in electro-Fenton reaction were monitored using transmission electron microscopy, indicating that the etching of MoS_2 nanosheets induced by hydroxyl radicals resulted in rapid homogeneous fracturing of the sheets into small dots via a transition of nanoporous morphology. The as-generated dots with the vertical dimensional thickness of ca. 0.7 nm and plane size of ca. 5 nm were demonstrated to be MoS_2 quantum dots (MoS_2-QDs) and their photoluminescence properties were explored based on the quantum confinement, edge effect, and intrinsic characteristics. Moreover, the degree of etching and the concomitant porosity of MoS_2 nanosheets could be conveniently tuned by electro-Fenton reaction time and a new morphology, nanoporous MoS_2 nanosheets, was obtained, raising new issues concerning MoS_2 nanosheets applications in various significant areas.

Introduction

Two-dimensional (2D) nanomaterials, derived from layered bulk crystals analogous to graphite, have aroused a great deal of consideration, because of their unusual properties associated with ultra-thin thickness and 2D morphology.[1-4] These developments have been spearheaded by researches of graphene, a 2D nanomaterial that is unique due to its combination of thermal, electronic, optical, and mechanical properties.[5-10] With the penetration of graphene, other 2D materials with a nano-layered structure such as hexagonal boron nitride, transition metal dichalcogenides, and metal halides have also attracted a large amount of interest.[11,15] Especially, MoS_2 nanosheets, 2D transition metal dichalcogenides, were obtained through efficient exfoliation of three-dimensional crystals and breaking the van der Waals interactions between nanosheets.[16-19] Owing to the specific 2D confinement of electron motion and absence of interlayer perturbation, the MoS_2 nanosheets possess a direct band gap and show some remarkable properties offering new opportunities in various areas, such as sensors,[18-22] single-layer transistors,[17] integrated circuits,[23] phototransistors,[24] nanometer thick photovoltaics,[25] and materials of batteries.[26,27] Recently, MoS_2 nanosheets were found to be promising materials for hydrogenation catalysis, attributed to active sites located along the edges of their layered crystal structure.[28-31] To achieve the potential applications of MoS_2 nanosheets limited by the insufficient active sites, defect-rich MoS_2 nanosheets,[29] oxygen-incorporated MoS_2 nanosheets,[30] and metallic MoS_2 nanosheets [31] representing some novel morphologies of MoS_2 nanosheets were presented.

Following the research of 2D and one-dimensional materials, zero-dimensional materials obtained more and more consideration. When compared to graphene sheets, zero-dimensional graphene quantum dots (GQDs) possess strong quantum confinement and edge effects, which induce new physical properties.[32] Due to their excellent properties and ongoing applications, the preparation of GQDs has been highly demanded and several strategies have been developed so far, such as hydrothermal route,[33] wave-assisted hydrothermal method,[34] ultrasonication breaking,[35] enzymatic oxidations,[36] steam etching,[37] and size fractionation.[38] Nevertheless, the mass scale manufacture of GQDs is limited by the harsh conditions, time consumption, low yield, and damage of aromatic carbon framework. To develop effective strategies for GQDs preparation, Fenton reaction with the assistance of ultraviolet light irradiation (photo-Fenton reaction) was proposed based on the etching of graphene oxide (GO).[39] However, regardless of conventional Fenton and photo-Fenton reaction, the initial addition of numerous Fe^{2+} and H_2O_2 makes an over-fast reaction occur in the beginning. Following the reaction, the consumption of Fenton reagent makes the rate of reaction down, which is detrimental to control the reaction rate and effectively prepare GQDs. Decades ago, electrochemically induced Fenton (electro-Fenton) reaction, an important advanced oxidation technology, was proposed and mainly used to the available degradation of pollutants in environment via generating highly powerful chemical oxidants hydroxyl radicals.[40] Electro-Fenton process is an attractive

method owing to its high effectiveness, fast treatment rate, and environmental compatibility in which hydrogen peroxide is generated in situ and the addition of ferrous ions allows an enhancement of the oxidation activity according to the following Fenton reaction through formation of •OH. Meanwhile, the ferrous ions are re-generated at the cathode, making the hydroxyl radicals be produced in a catalytic and controlled mode, tuned by a electrochemical process.[40]

So far, most attention is focused on the preparation, application, and property studies of MoS_2 nanosheets, leading to the relevant exploration of MoS_2 quantum dots (MoS_2-QDs) be ignored. Zero-dimensional MoS_2-QDs, owning the smaller plane size than MoS_2 nanosheets, possess strong quantum confinement and edge effects, which can induce numerous unique and outstanding properties. With the successful preparation of graphene quantum dots (GQDs) from the morphologic change of 2D graphene sheets,[33-39] MoS_2 nanosheets owing the specific 2D structure similar to graphene were also taken into consideration to prepare MoS_2-QDs. Herein, a simple, cost-effective, efficient,and controllable method for the production of hydroxyl radicals was used to cut GO into GQDs based on electro-Fenton reaction. Meanwhile, the reaction between MoS_2 nanosheets and hydroxyl radicals was explored, indicating the generation of zero-dimensional MoS_2-QDs from the etching of MoS_2 nanosheets (Scheme 1). The whole process of reaction was monitored by transmission electron microscopy (TEM) and a new MoS_2 nanosheets morphology, nanoporous MoS_2 nanosheets, was obtained via tuning the reaction time to control the degree of etching and concomitant porosity. Compared to MoS_2 nanosheets, both MoS_2-QDs and nanoporous MoS_2 nanosheets can provide much more active sites at the edge of plane, taken into a great deal of consideration for MoS_2 nanomaterials applications in various areas.

Experimental Section

Materials

Molybdenum(IV) sulfide (MoS_2 crystalline powder, < 2 μm, 99%) was purchased from Sigma-Aldrich Co., USA. Graphite powder (99.85%) was obtained from Shanghai Huayuan Chemical Engineering Co., Ltd., Shanghai, China. Sodium cholate (98%) and iron(II) sulfate heptahydrate ($FeSO_4 \cdot 7H_2O$) were purchased from Aladdin Chemistry Co., Ltd., Shanghai, China. Other chemicals employed in this work were of analytical reagent grade and purchased from Kelong Chemical Reagent Co., Ltd., Chengdu, China.

Experimental instrumentations

All electrochemical processes were conducted using a CHI 660B electrochemical workstation (CHEN HUA Instruments Co., China). A three-electrode system consisting of a 5 cm^2 graphite sheet working electrode, a saturated calomel electrode (SCE), and an auxiliary electrode made of platinum was adopted. All potentials were given with respect to the SCE. The KQ-250B ultrasonic bath (250 W, Kun Shan Ultrasonic Instruments Co., Ltd, China) was adopted to exfoliate MoS_2 powder. TEM, high resolution TEM (HRTEM), and high-angle annular dark-field scanning TEM (HAADF-STEM) measurements were performed on a Tecnai G2 F20 S-TWIN transmission electron microscope (FEI, USA) operated at 200 kV. The samples were prepared by dropping the aqueous suspension of GQDs and MoS_2 nanomaterials on the carbon grids and drying under ambient condition. Scanning electron microscope (SEM) images were obtained using an S-4800 field emission scanning electron microscope (Hitachi, Japan). Atomic force microscope (AFM) data were obtained on a Dimension Icon atomic force microscope (Bruker, Germany). X-ray diffraction (XRD) patterns were obtained with a D8 DISCOVER X-ray diffractometer (Bruker, Germany). UV-visible spectra were recorded on a UV-2450 UV-vis spectrophotomer (Shimadzu, Japan) at room temperature. The photoluminescence (PL) and photoluminescence excitation (PLE) spectra were recorded on an F-2700 fluorescence spectrophotometer (Hitachi, Japan) with Xe lamp as an excitation source; slit: 10 nm; PMT voltage: 400 V. The centrifugation was carried out using a TGL-16M high-speed refrigerated centrifuge (Xiangyi, China).

Preparation of MoS_2nanosheets and graphene oxide

MoS_2 nanosheets were prepared through the sonication-assisted exfoliation of MoS_2 crystal in aqueous surfactant solution.[41] A mixed water solution, containing 5 mg mL^{-1} MoS_2 powder and 1.5 mg mL^{-1} sodium cholate, was sonicated (KQ-250B 250 W) at normal temperature for 10 h, making the preparation of black dispersion. The dispersion was centrifuged at 3000 rpm for 30

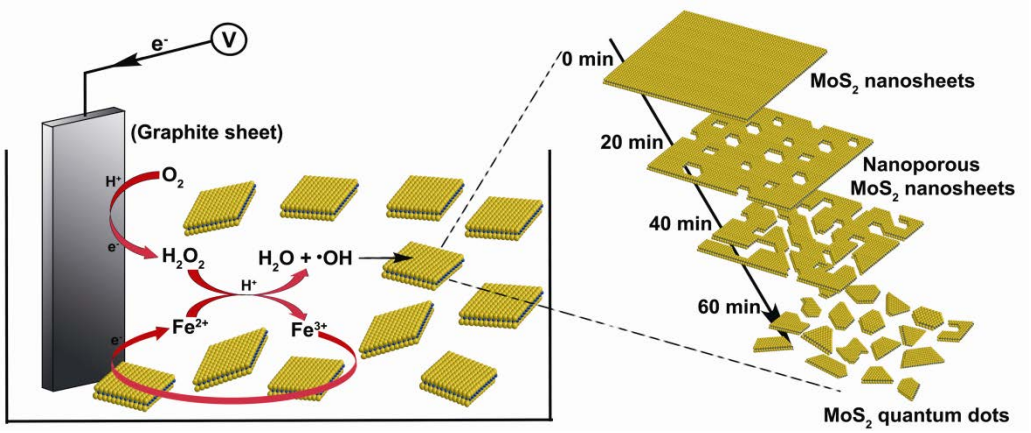

Scheme 1. Schematic illustration of the preparation of nanoporous MoS_2 nanosheets and MoS_2 quantum dots from electro-Fenton process.

min, followed by the separation of yellow-green supernatant to remove bulk MoS_2 powder. Furthermore, the separated supernatant was centrifuged at 12000 rpm for 30 min, making as-exfoliated MoS_2 nanosheets be obtained. To remove sodium cholate, the MoS_2 nanosheets were dispersed in ultrapure water with the assistance of sonication. Similarly, the regenerated dispersion was centrifuged at 12000 rpm for 30 min, followed by the collection of sediments to complete the washing process. The washing process was repeated for other two times to remove sodium cholate completely. Ultimately, the sediments were dispersed in a certain amount of ultrapure water to prepare uniform MoS_2 nanosheets dispersion. Graphene oxide was synthesized by the oxidation of graphite powder according to the hummers method and characterized in our pervious work.[42]

Electro-Fenton reaction

The electro-Fenton reaction of MoS_2 nanosheets (or graphene oxide) was conducted in an electrolytic cell equipped with an electrochemical workstation. A three-electrode system was adopted to connect the electrolytic cell with electrochemical workstation. A portion of 50 mL mixed solution containing 0.3 mg mL^{-1} exfoliated MoS_2 nanosheets (or graphene oxide) and 0.05 M $FeSO_4$ was added into the electrolytic cell. The initial pH of the mixture was adjusted to 3 by the dropwise addition of 0.5 M H_2SO_4 solution and it remained almost constant over the whole reaction. The potential of -0.5 V was applied and continuous saturation of the solution by O_2 at atmospheric pressure was ensured through bubbling of compressed air. Solutions were continuously stirred using a magnetic bar (500 rpm) to allow mass transfer. After various reaction times, the production was collected and dialyzed (Mw = 3500) in H_2SO_4 solution (pH = 3) for one day to remove iron ions and some other impurities, avoiding the production of sediments induced by hydrolysis of iron, and in ultrapure water for another day to remove H^+ and SO_4^{2-} ions.

Results and Discussion

Electro-Fenton process of graphene oxide

In electro-Fenton process, the electrochemical generation of H_2O_2 takes place at the cathode based on Equation 1 and with the addition of a certain amount of ferrous ions, the Fenton reagent thus formed leads to the formation of ·OH according to Equation 2.

$$O_2 + 2e^- + 2H^+ \rightarrow H_2O_2 \quad (1)$$

$$Fe^{2+} + H_2O_2 + H^+ \rightarrow Fe^{3+} + \cdot OH + H_2O \quad (2)$$

Meanwhile, O_2 is fed into the electrochemical system making the concentration of H_2O_2 keep almost constant (Fig. S1). The regeneration of Fe^{2+} can occur by a direct cathodic reaction (Equation 3) under the conditions of electro-generation of H_2O_2, and contribute to further production of a great number of hydroxyl radicals.

$$Fe^{3+} + e^- \rightarrow Fe^{2+} \quad (3)$$

Compared to conventional Fenton and photo-Fenton reaction, electro-Fenton reaction can be conveniently controlled by tuning the electrochemical process, making the generation of hydroxyl radicals more efficient and controllable. The controllability of electro-Fenton process was confirmed through conducting the experiment about the degradation of rhodamine B (Fig. S2). Meanwhile, when a specific condition for electro-Fenton process was confirmed, the impact of •OH on the substrate only depended on the reaction time.

Hydroxyl radicals-mediated oxidation of aromatic molecules has been established before. The initial attack of hydroxyl radical produces an •OH adduct or undergoes electron transfer to produce cation radicals and continued attack of hydroxyl radicals causes complete oxidation of aromatic molecules to CO_2 and water. Graphene and GO sheets could be considered as super aromatic molecules and the reaction between graphene sheets and hydroxyl radicals has been discussed.[39,43] The hydroxyl radicals can make an impact on aromatic molecules and further break up parts of the hexatomic ring structure of GO sheets. On the basis of the exploration about electro-Fenton process, the route that using electro-Fenton process to prepare GQDs from GO was proposed. Under the optimal conditions (Fig. S3), the electro-Fenton process of GO was conducted and the progresses were monitored using AFM. From the results (Fig. S4), it was obviously observed that bulk GO sheets turned into a great deal of small dots possessing a vertical dimensional thickness of ca. 0.8 nm after reaction for 60 min, which were demonstrated to be GQDs with great photoluminescence properties. As shown in the TEM image (Fig. 1a), the plane sizes of as-prepared GQDs are uniform, ranging from 1.6 to 4.0 nm with the average value of approximately 2.53 nm. The lattice spacing of the GQDs (plane size: ca. 2.60 nm) in the HRTEM image (Fig. 1b) is ca. 2.14 Å, which is similar to the hexagonal pattern of graphene with d_{1100}.[44] It was confirmed that hydroxyl radicals generated from electro-Fenton process could break the 2D structure of GO and played a positive impact on the conversion of GO to GQDs. In electro-Fenton reaction, the rates of hydroxyl radical production were influenced by electrochemical process, making it effective to control the whole process of GQDs preparation. The UV-vis spectra of GO before and after the electro-Fenton reaction were recorded. As shown in Fig. S5, the GO has two absorption peaks at 230 and 304 nm, corresponding to π to π * transition of aromatic sp^2 domains and n to π * transition of C=O bond, respectively. Meanwhile, two UV-vis absorption peaks centered at 210 and 276 nm are observed after GO solution reacted with the electro-Fenton reagent (Fig. S5). The origin of these absorptions can be ascribed to π electron transition in oxygen-containing GQDs. The stronger absorption at 210 nm corresponds to a good deal of π to π * transition of aromatic sp^2 domains, and the absorption at 276 nm is due to n to π* transition of C=O bond, located in the edge of GQDs.[33] The PL and PLE spectra of the GQDs solution were recorded (Fig. 1c). The GQDs were excited by a Xe lamp from the fluorescence spectrometer and an optimal emission peak centered at 401 nm was observed when the sample was excited at 320 nm with a Stokes shift of 81 nm. The PLE spectrum recorded with the optimal luminescence showed two peaks at 256 nm, which was regarded as a shoulder peak, and 320 nm. The theory used to account for this phenomenon was proposed by Pan et al.[33] The PLE peaks at 256 and 320 nm correspond to the absorption from the transitions of π to π* and n to π*, related to the absorption peaks at 210 and 276 nm in absorption spectrum, respectively. Furthermore, the PLE spectrum demonstrates that the luminescence observed from GQDs is directly correlated with both of the two kinds of transitions rather than only transition of π to π*, which can be used to explain the unique optical properties of GQDs. The as-

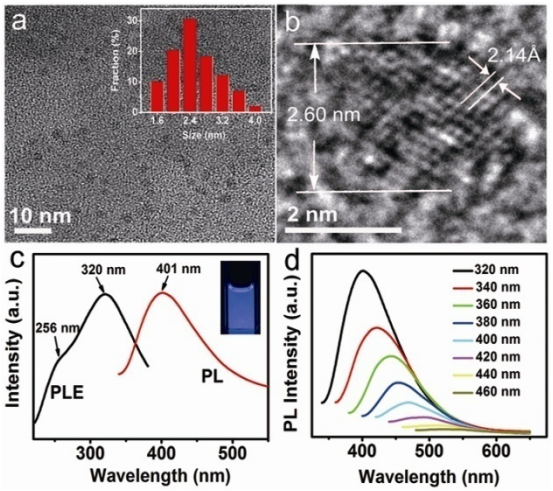

Fig. 1 (a) TEM image of the GQDs prepared from electro-Fenton reaction and diameter distribution of as-prepared GQDs. (b) HRTEM image of an individual GQD shown in panel a. (c) PLE spectra of GQDs with the detection wavelength of 401 nm and PL spectra excited at 320 nm. (d) PL spectra of the GQDs excited by various wavelengths ranging from 320 to 460 nm.

prepared GQDs also exhibits an excitation-dependent PL behavior. When the excitation wavelength changes from 320 to 460 nm, the PL peak shifts to longer wavelengths and the PL intensity decreases significantly (Fig. 1d).

With the successful preparation of GQDs from morphologic change of GO sheets induced by hydroxyl radicals in electro-Fenton reaction, it was proposed that other 2-dimensional materials like graphene in structure might react with hydroxyl radicals as well. Therefore, due to the unique and excellent properties, few-layer MoS_2 nanosheets, originally obtained from exfoliation of MoS_2 powder, were also taken into consideration. To the best of our knowledge, the discussion about the reaction between MoS_2 nanosheets and hydroxyl radicals has never been conducted before. Nevertheless, the morphologic changes of MoS_2 nanosheets under the influence of hydroxyl radicals generated from electro-Fenton reaction attracted our interests.

Exfoliation of MoS_2 in aqueous surfactant solution

A more recent strategy for exfoliation is to expose the layered material to ultrasonic waves in a solvent.[41,45] Such waves generate cavitation bubbles that collapse into high-energy jets, breaking up the layered crystallites and producing exfoliated nanosheets. Sonication has been used to exfoliate bulk MoS_2 in water, so long as ionic surfactants are present to prevent rapid reaggregation of MoS_2 nanosheets due to their van der Waals binding to the exfoliated sheets and subsequent electrostatic stabilization.[41] In our experiment, MoS_2 nanosheets were obtained through the sonication-assisted exfoliation of MoS_2 crystal in aqueous surfactant solution (Fig. 2a). MoS_2 powder was added to sodium cholate aqueous solution for sonication-treatment, resulting in the preparation of dispersed solution. Centrifugation of dispersed solution at 3000 rpm was used to remove the bulk and thicker MoS_2. The precipitation was collected at 12000 rpm to obtain exfoliated MoS_2 nanosheets. The surfactant adsorbed on the surface of MoS_2 nanosheets was removed through re-dispersing the precipitation in ultrapure water and collecting the new precipitation at 12000 rpm in centrifugation. The results of thermogravimetric analysis were used to verify the purification of MoS_2 nanosheets through the process of washing and centrifugation, exhibiting that most of sodium cholate were removed (Fig. S6). Optical absorption is one characteristic which is related to the band structure of a semiconductor. Bulk MoS_2 is a semiconductor with an indirect bandgap of about 1.29 eV and no characteristic absorption peak can be observed in UV-vis absorption spectrum.[16] However, theoretical calculation has predicted an indirect to direct bandgap transition in the *d*-electron system when the bulk MoS_2 is thinned to a single layer, and the few angstrom-thin single-layered MoS_2 has recently been reported to exhibit a significant energy bandgap of 1.8 eV, while those of double- and triple-layer MoS_2 reduce to 1.65 and 1.35 eV, respectively.[46] The as-exfoliated MoS_2 nanosheets aqueous solution with yellow-green color has two characteristic absorption peaks at 610 and 672 nm (Fig. 2b), corresponding to B and A excitonic peaks, respectively, derived from the K point of the Brillourin zone in 2D MoS_2 with large lateral dimensions.[25,45] The sheet structure and morphology are obviously exhibited in SEM image (Fig. 2c), primarily showing the nanoscale of as-exfoliated MoS_2. The AFM image of MoS_2 nanosheets is shown in Fig. 2d and the height of as-exfoliated MoS_2 nanosheets was measured to be around 2.8 nm (Inset of Fig. 2d), corresponding to about 4 monolayers of MoS_2.[25,47] A statistical analysis based on AFM measurements indicated that the MoS_2 nanosheets prepared from sonication-assisted exfoliation of MoS_2 powder had various thicknesses with the

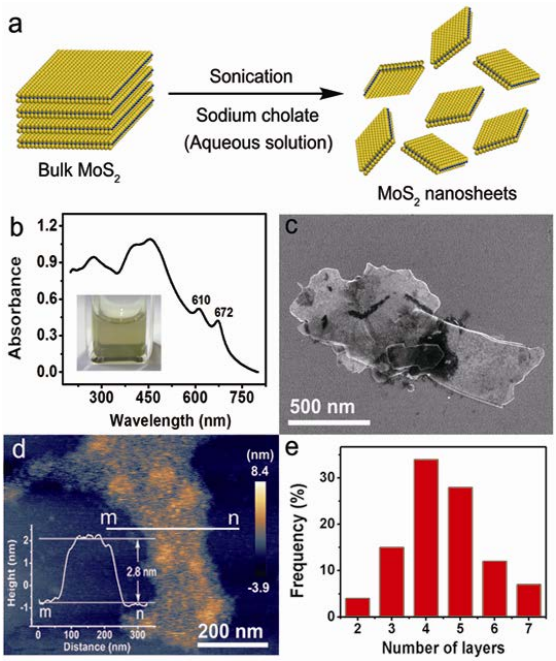

Fig. 2 (a) Schematic illustration of the exfoliation of bulk MoS_2 for the preparation of MoS_2 nanosheets. (b) UV-vis absorption spectrum and photograph (inset) of exfoliated MoS_2 nanosheets aqueous solution. (c) SEM and (d) AFM images of a typical MoS_2 nanosheet with the inset representing the height profile along the white line overlaid on the image. (e) The thickness distribution based on 100 randomly selected MoS_2 nanosheets.

majority in the range of 3 to 5 monolayers (Fig. 2e).

During the past few years, MoS_2 based catalysts have been considered promising alternatives for platinum due to their high abundance and low cost. Promising catalytic activity from MoS_2 in the hydrogen evolution reaction (HER) is attributed to the active site located along the edges of its two-dimensional layered crystal. If MoS_2 based catalysts are to realize their potential, there is an urgent need to design MoS_2 nanostructures with more edge sites.[28-31] On the basis of electro-Fenton reaction of GO turning 2D graphene sheets into small quantum dots, the protocol that using electro-Fenton reaction to generate new morphologies of MoS_2 sheets was proposed.

Electro-Fenton process of MoS_2 nanosheets

The progresses of electro-Fenton reaction of MoS_2 nanosheets were monitored using TEM. As shown in Fig. 3a, the basal plane of MoS_2 nanosheets is clearly observed, meanwhile, a number of ultrasmall nanoparticles, representing the fragments arising from sonication of bulk crystals, could also be found in the samples of as-obtained nanosheets. After 20 min of the reaction, a few small holes with a diameter of approximately 20 nm are distinctly observed on the basal plane of MoS_2 nanosheets (Fig. 3b). Undergoing a short time of electro-Fenton reaction less than 20 min, the layered morphology of the MoS_2 nanosheets is still preserved, but exhibits the nanoporous facets. Herein, a new morphology of MoS_2, nanoporous MoS_2 nanosheet, was obtained through electro-Fenton treatment of exfoliated MoS_2 nanosheets. Indeed, considerable focus has been placed in developing unique morphologies of 2D material, including graphene sheets with nanoporous facets that exhibit excellent performance as supercapacitor electrodes.[48,49] By creating pores within the MoS_2 nanosheets, the active edge sites at the surface of sheets can increase and improvements in some unique properties of MoS_2 nanosheets are realized. Similar to the nanoporous graphene sheets, the nanoporous MoS_2 nanosheets should exhibit potential use in opto-electronic and renewable energy applications. Furthermore, with the reaction time increasing to 40 min, an increasing number of holes with various sizes appeared on the MoS_2 nanosheets, and a number of small nanosheets under the quantum scale were gradually obtained, which were derived from the spaces between holes (Fig. 3c). After 60 min of the electro-Fenton reaction, MoS_2 nanosheets were completely cut into small dots (Fig. 3d), which were demonstrated to be zero-dimensional MoS_2-QDs later using HRTEM, AFM, and PL. As a control experiment, the same electrochemical process of MoS_2 nanosheets aqueous solution without the addition of Fe^{2+} was conducted for 60 min, and no apparent changes were found on basal planes. Meanwhile, the reaction of MoS_2 nanosheets with conventional Fenton reagent was carried out, and no any apparent holes or changes were observed. It was verified that electrochemical process and pre-Fenton reagents (O_2 and Fe^{2+}) were essential for the preparation of nanoporous MoS_2 monosheets and MoS_2-QDs.

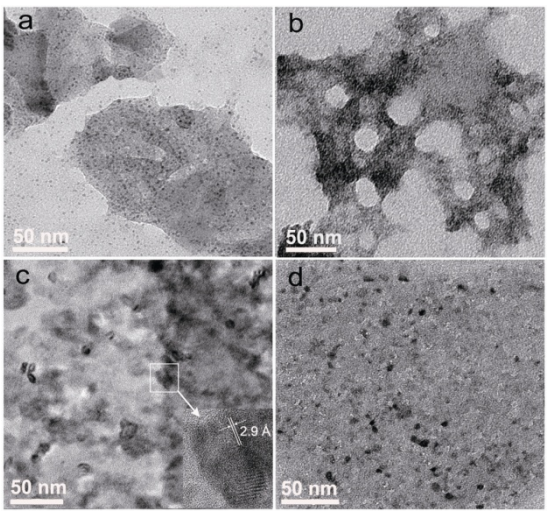

Fig. 3 TEM images of MoS_2 nanosheets before (a) and after being reacted with the pre-Fenton reagents (O_2 and Fe^{2+}) under the assistance of electrochemical process (applied potential of -0.5 V) for 20 (b), 40 (c), and 60 (d)min, respectively. The inset in Figure 3c is the HRTEM image of single MoS_2-QD shown in panel c.

Characterization of MoS_2 quantum dots

The as-prepared MoS_2-QDs were subjected to TEM measurement (Fig. 4a), revealing that a few MoS_2-QDs are uniformly distributed without agglomeration. The HRTEM image (Fig. 4b) shows an individual MoS_2 quantum dot with the length and width of approximately 11.5 and 5.3 nm, respectively, indicating that zero-dimenional MoS_2-QDs have a different morphology compared with other one-dimenional nanomaterials, such as

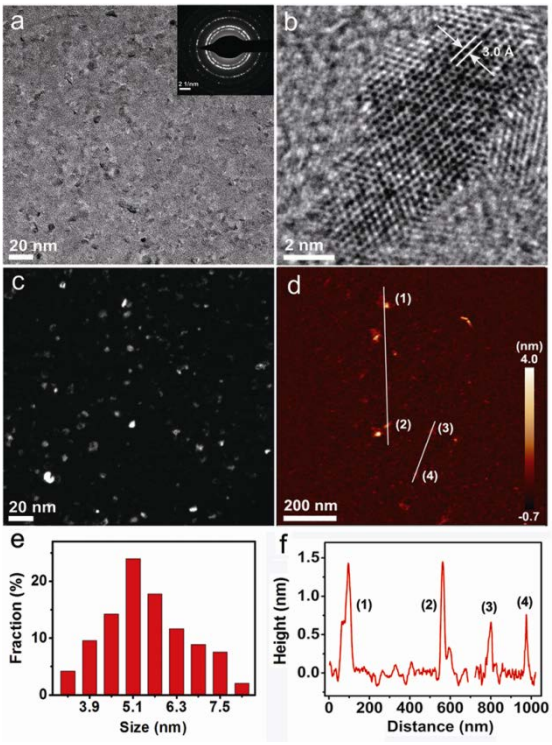

Fig. 4 (a) TEM image of the as-prepared MoS_2-QDs and the inset presents a typical electron diffraction pattern of MoS_2-QDs. (b) HRTEM image of an individual MoS_2-QD with measured lattice spacing. (c) HAADF-STEM image of the dots. (d) AFM image of the dots deposited on freshly cleaved mica substrates. (e) Size distribution and (f) height distribution of as-prepared MoS_2-QDs in panel d. Height: ca. 0.7 nm, one layer; ca. 1.4 nm, two layers.

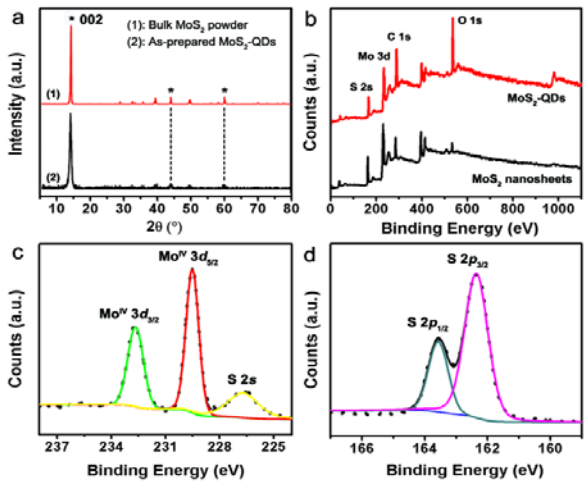

Fig. 5 (a) XRD patterns of MoS_2-QDs prepared from electro-Fenton reaction and bulk MoS_2 powder (peaks correspond to [*] 2H MoS_2). (b) XPS survey of MoS_2 nanosheets before electro-Fenton reaction and as-prepared MoS_2-QDs. High resolution Mo 3d (c) and S 2p (d) spectra of MoS_2-QDs.

nanoribbon, nanotube, and nanowire.[50] Moreover, as expected, the HRTEM illustrates that the MoS_2-QDs have 2D hexagonal symmetry crystalline structure with the lattice spacing of 3.0 Å, which is similar to the hexagonal pattern of MoS_2 monolayer.[51] This result was further verified by the electron diffraction pattern of MoS_2-QDs (Inset of Fig. 4a). In order to reveal the morphology feature of MoS_2-QD, HAADF-STEM image is shown clearly in Fig. 4c. Fig. 4d presents the AFM image of the MoS_2-QDs on a flesh mica substrate and a few small dots with various scales of heights below 3 nm are observed. From the size distribution (Fig. 4e), we can see that the size of as-prepared MoS_2-QDs was uniform ranging from 3 to 8 nm with the average value of 5.43 nm. Meanwhile, combining the AFM image and height distribution (Fig. 4f), it was shown that the heights of most of the MoS_2-QDs were below 2 nm, that is, around 1.4 nm representing the height of MoS_2 bilayers and approximately 0.7 nm indicating the type of monolayer.

The crystal structure of these as-generated MoS_2-QDs is investigated using XRD system, while the MoS_2 powder is used as the reference. From the XRD pattern shown in Fig. 5a, it can be observed that both MoS_2-QDs and bulk powder are identified as 2H MoS_2 with a dominant peak appearing at 14.4°, representing the (002) plane (ICDD card no. 77-1716).[52] In order to explore the changes of chemical composition, XPS of MoS_2 nanosheets before and after electro-Fenton reaction were recorded. It can be seen from Fig. 5b that XPS survey exhibits that the proportion of oxygen element in MoS_2 nanosheets sample after electro-Fenton reaction increases due to the influence of hydroxyl radicals. Meanwhile, the atomic ratio of Mo:S increase from 1:2.30 (MoS_2 nanosheets) to 1:2.42 (MoS_2-QDs), ascribed to an increasing number of unsaturated sulfur atoms located at the external edge of MoS_2-QDs. As shown in Fig. 5c and 5d, $Mo3d_{3/2}$, $Mo3d_{5/2}$, S2s, $S2p_{1/2}$, and $S2p_{3/2}$ peaks can be observed at 232.7, 229.5, 226.7, 163.6, and 162.3 eV, respectively, indicating the dominant 2H MoS_2 phase in the crystal structure.[52] Two characteristic peaks located at 229.5 and 232.7 eV arise from Mo $3d_{5/2}$ and Mo $3d_{3/2}$, suggesting the dominance of +4 oxidation state.[30] Whereas the S 2p region (Fig. 5d) exhibits primarily a single doublet with the $2p_{3/2}$ peak at 162.3 eV, corresponding to -2 oxidation state of sulfur.[30] The semiconducting phase of as-prepared MoS_2-QDs (2H MoS_2) was further verified based on the XPS analyses.

Photoluminescence properties of MoS_2 quantum dots

Recent success in isolating MoS_2 monolayer has allowed the observation of strong photoluminescence, attributed to the direct gap electronic structure of monolayer MoS_2. According to theoretical calculation,[53,54] the MoS_2 nanostructure exhibited some unique photoluminescence properties due to the effect of quantum confinement and edge. Therefore, the optical properties of as-prepared MoS_2-QDs were explored. Fig. 6a shows the PL spectra of exfoliated MoS_2 nanosheets solutions at different reaction times in electro-Fenton process when the excitation wavelength is 283 nm. It can be seen that the as-exfoliated MoS_2 nanosheets before the electro-Fenton reaction are PL inactive, indicating the absence of MoS_2-QDs in exfoliated MoS_2 nanosheets samples. However, after 20 min of electro-Fenton reaction, the as-generated nanoporous MoS_2 nanosheets (Fig. 3b) show weak PL peak centered at 370 nm, which continues to increase when the reaction time increases to 60 min. Hence, the morphology of quantum dot (Fig. 3d) was demonstrated to exhibit great PL property. The MoS_2-QDs have an absorption band peaked at 276 nm (Fig. 6b), whereas the characteristic absorption peaks of exfoliated MoS_2 nanosheets at 610 and 672 nm disappeared, indicating the absence of 2D MoS_2 nanosheets with large lateral dimensions in as-prepared MoS_2-QDs. It was suggested that the optical absorption of low-dimensional or

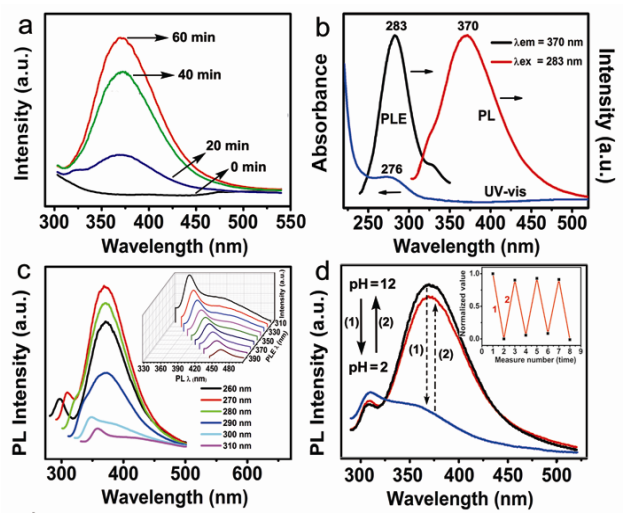

Fig. 6 (a) PL spectra of exfoliated MoS_2 nanosheets suspensions before and after the electro-Fenton reaction for 20, 40, and 60 min using the excitation wavelength of 283 nm. (b) UV-vis absorption, PL, and PLE spectra of MoS_2-QDs dispersed in water. (c) PL spectra of as-prepared MoS_2-QDs aqueous solution at different excitation wavelengths ranging from 260 to 310 nm. Inset: excitation wavelengths ranging from 310 to 390 nm. (d) pH-dependent PL spectra when pH is switched between 12 and 2. Inset: reversible switching of PL intensity through the change of pH between 12 and 2.

quantum dot MoS_2 exhibited a strong blue shift when the lateral dimensions of the MoS_2 nanostructures were reduced to <50 nm, ascribed to the quantum size effect.[52] Hence, for MoS_2-QDs with the plane size of ca. 5 nm, the optical absorption peak centered at 276 nm can be assigned to blue-shifted convoluted Z, C, and D excitonic peaks.[52,55] As we can see from the PL and PLE spectra (Fig. 6b), an optimal emission peak centered at 370 nm is observed when the sample is excited at 283 nm with a Stokes shift of 87 nm. The PLE spectrum recorded with the detection wavelength of 370 nm shows a peak at 283 nm, corresponding to the absorption peak at 276 nm in the UV-vis absorption spectrum. The PL spectra excited by different wavelengths ranging from 260 nm to 390 nm were recorded in Fig. 6c, showing that MoS_2-QDs aqueous solution have an excitation-independent characteristic emission spectrum peaked at 370 nm and the PL intensity decreases with the excitation wavelengths changing from 270 to 310 nm. Meanwhile, there is another weaker emission spectrum being observed. When the excitation wavelength changes from 270 to 390 nm, the PL peak shifts to longer wavelengths peaked from 310 to 465 nm and the intensity decreases, showing the excitation-dependent characteristic. A pH-dependent PL with the peak at 370 nm is exhibited in MoS_2-QDs aqueous solution (Fig. 6d). Under alkaline conditions, the MoS_2-QDs emit strong PL, whereas, the PL is nearly completely quenched under acidic conditions. If pH is switched repeatedly between 12 and 2, the PL intensity varies reversibly. It has been suggested that a significant number of H^+ intercalates into the 2H MoS_2-QDs, transforming it from the semiconducting 2H phase into the metallic MoS_2 (1T) phase that eventually leads to the loss of their PL properties.[47]

Conclusion

In summary, a new route to effectively and controllably prepare GQDs from GO sheets was proposed using electro-Fenton reaction. Meanwhile, it was demonstrated that the exfoliated MoS_2 nanosheets could react with hydroxyl radicals induced by electro-Fenton process, achieving the generation of new morphologies, nanoporous MoS_2 nanosheets, and zero-dimensional MoS_2-QDs, in a mass scale. The as-prepared MoS_2-QDs showed unique PL properties due to the quantum confinement, edge effect and their intrinsic characteristics, which were of great promise to be a novel optical probe and used for optoelectronic systems. Compared to MoS_2 nanosheets exhibiting excellent catalytic activity for the hydrogen evolution reaction, nanoporous MoS_2 sheets and MoS_2 quantum dots possessing much more active edge sites could enable new opportunities for enhancing properties in hydrogen evolution catalysis and other important technological applications.

Acknowledgements

This work was supported by the National Natural Science Foundation of China (Nos. 20975083 and 21273174) and the Municipal Science Foundation of Chongqing City (No. CSTC-2013jjB00002).

Notes and references

[a] *Key Laboratory of Eco-environments in Three Gorges Reservoir Region (Ministry of Education), School of Chemistry and Chemical Engineering, SouthwestUniversity, Chongqing 400715, P.R. China. Fax: +86-23-68253237. Tel: +86-23-68253237. E-mail: linb@swu.edu.cn (N. B. Li); luohq@swu.edu.cn (H. Q. Luo).*

[b] *School of Chemistry and Chemical Engineering, Chongqing University, Chongqing 400044, P.R. China.*

† Electronic Supplementary Information (ESI) available: Fig. S1 to Fig. S6. See DOI: 10.1039/b000000x/

1 X. Huang, Z. Zeng and H. Zhang, *Chem. Soc. Rev.*, 2013, **42**, 1934.
2 K. Xu, P. Chen, X. Li, C. Wu, Y. Guo, J. Zhao, X. Wu and Y. Xie, *Angew. Chem. Int. Ed.*, 2013, **52**, 10477.
3 H. Li, J. Wu, Z. Yin and H. Zhang, *Acc. Chem. Res.*, 2014, **47**, 1067.
4 V. Nicolosi, M. Chhowalla, M. G. Kanatzidis, M. S. Strano and J. N. Coleman, *Science*, 2013, **340**, 1226419.
5 R. C. Haddon, *Acc. Chem. Res.*, 2013, **46**, 2191.
6 X. Huang, Z. Zeng, Z. Fan, J. Liu and H. Zhang, *Adv. Mater.*, 2012, **24**, 5979.
7 Q. He, S. Wu, Z. Yin and H. Zhang, *Chem. Sci.*, 2012, **3**, 1764.
8 A. K.Geim, *Science*, 2009, **324**, 1530.
9 A. K. Geimand, K. S. Novoselov, *Nat. Mater.*, 2007, **6**, 183.
10 H. Jiang, *Small*, 2011, **7**, 2413.
11 Y. Zhao, X. Luo, H. Li, J. Zhang, P. T. Araujo, C. K. Gan, J. Wu, H. Zhang, S. Y. Quek, M. S. Dresselhaus and Q. Xiong, *Nano Lett.*, 2013, **13**, 1007.
12 S. Z. Butler, S. M. Hollen, L. Cao, Y. Cui, J. A. Gupta, H. R. Gutierrez, T. F. Heinz, S. S. Hong, J. Huang, A. F. Ismach, E. Johnston-Halperin, M. Kuno, V. V. Plashnitsa, R. D. Robinson, R. S. Ruoff, S. Salahuddin, J. Shan, L. Shi, M. G. Spencer, M. Terrones, W. Windl and J. E. Goldberger, *ACS Nano*, 2013, **7**, 2898.
13 X. Huang, C. Tan, Z. Yin and H. Zhang, *Adv. Mater.*, 2014, **26**, 2185.
14 X. Huang, Z. Zeng, S. Bao, M. Wang, X. Qi, Z. Fan and H. Zhang, *Nat. Commum.*, 2013, **4**, 1444.
15 Z. Zeng, C. Tan, X. Huang, S. Bao and H. Zhang, *Energy Environ. Sci.*, 2014, **7**, 797.
16 K. F. Mak, C. Lee, J. Hone, J. Shan and T. F. Heinz, *Phys. Rev. Lett.*, 2010, **105**, 136805.
17 B. Radisavljevic, A. Radenovic, J. Brivio, V. Giacometti and A. Kis, *Nat. Nanotechnol.*, 2011, **6**, 147.
18 H. Li, Z. Yin, Q. He, H. Li, X. Huang, G. Lu, D. W. H. Fam, A. I. Y. Tok, Q. Zhang and H. Zhang, *Small*, 2012, **8**, 63.
19 Z. Zeng, Z. Yin, X. Huang, H. Li, Q. He, G. Lu, F. Boey and H. Zhang, *Angew. Chem. Int. Ed.*, 2011, **50**, 11093.
20 C. Zhu, Z. Zeng, H. Li, F. Li, C. Fan and H. Zhang, *J. Am. Chem. Soc.*, 2013, **135**, 5998.
21 Q. He, Z. Zeng, Z. Yin, H. Li, S. Wu, X. Huang and H. Zhang, *Small*, 2012, **8**, 2994.
22 S. Wu, Z. Zeng, Q. He, Z. Wang, S. J. Wang, Y. Du, Z. Yin, X. Sun, W. Chen and H. Zhang, *Small*, 2012, **8**, 2264.
23 B. Radisavljevic, M. B. Whitwick and A. Kis, *ACS Nano*, 2011, **5**, 9934.
24 Z. Yin, H. Li, H. Li, L. Jiang, Y. Shi, Y. Sun, G. Lu, Q. Zhang, X. Chen and H. Zhang, *ACS Nano*, 2012, **6**, 74.
25 M. Bernardi, M. Palummo and J. C. Grossman, *Nano Lett.*, 2013, **13**, 3664.
26 J. Xiao, D. Choi, L. Cosimbescu, P. Koech, J. Liu and J. P. Lemmon, *Chem. Mater.*, 2010, **22**, 4522.
27 Y. Liang, R. Feng, S. Yang, H. Ma, J. Liang and J. Chen, *Adv. Mater.*, 2011, **23**, 640.
28 J. Kibsgaard, Z. Chen, B. N. Reinecke and T. F. Jaramillo, *Nat. Mater.*, 2012, **11**, 963.
29 J. Xie, H. Zhang, S. Li, R. Wang, X. Sun, M. Zhou, J. Zhou, X. W. Lou and Y.Xie, *Adv. Mater.*, 2013, **25**, 5807.
30 J. Xie, J. Zhang, S. Li, F. Grote, X. Zhang, H. Zhang, R. Wang, Y. Lei, B. Pan and Y. Xie, *J. Am. Chem. Soc.*, 2013, **135**, 17881.
31 M. A. Lukowski, A. S. Daniel, F. Meng, A. Forticaux, L. Li and S. Jin, *J. Am. Chem. Soc.*, 2013, **135**, 10274.
32 L.A. Ponomarenko, F. Schedin, M. I. Katsnelson, R. Yang, E. W. Hill, K. S. Novoselov and A. K. Geim, *Science*, 2008, **320**, 356.
33 D. Pan, J. Zhang, Z. Li and M. Wu, *Adv. Mater.*, 2010, **22**, 734.
34 L. Tang, R. Ji, X. Cao, J. Lin, H. Jiang, X. Li, K. S. Teng, C. M. Luk,

S. Zeng, J. Hao and S. P. Lau, *ACS Nano*, 2012, **6**, 5102.
35 J. T. Robinson, S. M. Tabakman, Y. Liang, H. Wang, H. S. Casalongue, D. Vinh and H. Dai, *J. Am. Chem. Soc.*, 2011, **133**, 6825.
36 G. P. Kotchey, B. L. Allen, H. Vedala, N. Yanamala, A. A. Kapralov, Y. Y. Tyurina, J. Klein-Seetharaman, V. E. Kagan and A. Star, *ACS Nano*, 2011, **5**, 2098.
37 T. H. Han, Y. K. Huang, A. T. L. Tan, V. P. Dravid and J. Huang, *J. Am. Chem. Soc.*, 2011, **133**, 15264.
38 X. Wang, H. Bai and G. Shi, *J. Am. Chem. Soc.*, 2011, **133**, 6338.
39 X. Zhou, Y. Zhang, C. Wang, X. Wu, Y. Yang, B. Zheng, H. Wu, S. Guo and J. Zhang, *ACS Nano*, 2012, **6**, 6592.
40 S. Yuan, Y. Fan, Y. Zhang, M. Tong and P. Liao, *Environ. Sci. Technol.*, 2011, **45**, 8514.
41 R. J. Smith, P. J. King, M. Lotya, C. Wirtz, U. Khan, S. De, A. O'Neill, G. S. Duesberg, J. C. Grunlan, G. Moriarty, J. Chen, J. Wang, A. I. Minett, V. Nicolsi and J. N. Coleman, *Adv. Mater.*, 2011, **23**, 3944.
42 Y. Shi, W. T. Huang, H. Q. Luo and N. B. Li, *Chem. Commun.*, 2011, **47**, 4676.
43 J. G. Radich and P. V. Kamat, *ACS Nano*, 2013, **7**, 5546.
44 S. H. Jin, D. H. Kim, G. H. Jun, S. H. Hong and S. Jeon, *ACS Nano*, 2013, **7**, 1239.
45 J. N. Coleman, M. Lotya, A. O'Neill, S. D. Bergin, P. J. King, U. Khan, K. Young, A. Gaucher, S. De, R. J. Smith, I. V. Shvets, S. K. Arora, G. Stanton, H. Y. Kim, K. Lee, G. T. Kim, G. S. Duesberg, T. Hallam, J. J. Boland, J. J. Wang, J. F. Donegan, J. C. Grunlan, G. Moriarty, A. Shmeliov, R. J. Nicholls, J. M. Perkins, E. M. Grieveson, K. Theuwissen, D. W. McComb, P. D. Nellist and V. Nicolosi, *Science*, 2011, **331**, 568.
46 H. S. Lee, S. W. Min, Y. G. Chang, M. K. Park, T. Nam, H. Kim, J. H. Kim, S. Ryu and S. Im, *Nano Lett.*, 2012, **12**, 3695.
47 J. Z. Ou, A. F. Chrimes, Y. Wang, S. Tang, M. S. Strano and K. Kalantar-zadeh, *Nano Lett.*, 2014, **14**, 857.
48 L. L. Zhang, X. Zhao, M. D. Stoller, Y. Zhu, H. Ji, S. Murali, Y. Wu, S. Perales, B. Clevenger and R. S. Ruoff, *Nano Lett.*, 2012, **12**, 1806.
49 Y. Zhu, S. Murali, M. D. Stoller, K. J. Ganesh, W. Cai, P. J. Ferreira, A. Pirkle, R. M. Wallace, K. A. Cychosz, M. Thommes, D. Su, E. A. Stach and R. S. Ruoff, *Science*, 2011, **332**, 1537.
50 X. L. Xu, J. X. Wang, G. Y. Jing, Z. X. Shen, B. S. Zou, H. M. Fan and M. Olivo, *Nanoscale*, 2012, **4**, 5665.
51 K. Wang, J. Wang, J. Fan, M. Lotya, A. O'Neill, D. Fox, Y. Feng, X. Zhang, B. Jiang, Q. Zhao, H. Zhang, J. N. Coleman, L. Zhang and W. J. Blau, *ACS Nano*, 2013, **7**, 9260.
52 Y. Wang, J. Z. Ou, S. Balendhran, A. F. Chrimes, M. Mortazavi, D. D. Yao, M. R. Field, K. Latham, V. Bansal, J. R. Friend, S. Zhuiykov, N. V. Medhekar, M. S. Strano and K. Kalantar-zadeh, *ACS Nano*, 2013, **7**, 10083.
53 A. Splendiani, L. Sun, Y. Zhang, T. Li, J. Kim, C. Y. Chim, G. Galli and F. Wang, *Nano Lett.*, 2010, **10**, 1271.
54 Y. Li, Z. Zhou, S. Zhang and Z. Chen, *J. Am. Chem. Soc.*, 2008, **130**, 16739.
55 J. P. Wilcoxon and G. A. Samara, *Phys. Rev. B*, 1995, **51**, 7299.